Atmos. Chem. Phys. Discuss., 14, 31899–31942, 2014
www.atmos-chem-phys-discuss.net/14/31899/2014/
doi:10.5194/acpd-14-31899-2014

Atmospheric Chemistry and Physics Discussions
Open Access

Impacts of emission reductions on aerosol radiative effects

J.-P. Pietikäinen[1], K. Kupiainen[2,3], Z. Klimont[2], R. Makkonen[4], H. Korhonen[1], R. Karinkanta[1], A.-P. Hyvärinen[1], N. Karvosenoja[3], A. Laaksonen[1], H. Lihavainen[1], and V.-M. Kerminen[4]

[1]Finnish Meteorological Institute, P.O. Box 503, 00101, Helsinki, Finland
[2]International Institute for Applied Systems Analysis, Schlossplatz 1, 2361, Laxenburg, Austria
[3]Finnish Environment Institute SYKE, P.O. Box 140, 00251, Helsinki, Finland
[4]Department of Physics, University of Helsinki, P.O. Box 44, 00014, Helsinki, Finland

Received: 31 October 2014 – Accepted: 2 December 2014 – Published: 17 December 2014

Correspondence to: J.-P. Pietikäinen (joni-pekka.pietikainen@fmi.fi)

Published by Copernicus Publications on behalf of the European Geosciences Union.

Abstract

The global aerosol–climate model ECHAM-HAMMOZ is used to study the aerosol burden and forcing changes in the coming decades. Four different emissions scenarios are applied for 2030 (two of them applied also for 2020) and the results are compared against reference year 2005. Two of the scenarios are based on current legislation reductions, one shows the maximum potential of reductions that can be achieved by technical measures, and the last one is targeted to short-lived climate forcers (SLCFs). We have analysed the results in terms of global means and additionally focused on 8 sub-regions. Based on our results, aerosol burdens overall show decreasing trend, but in some locations, such as India, the burdens could increase significantly. This has impact on the direct aerosol effect (DRE), which could reduce globally 0.06–0.4 $\mathrm{W\,m^{-2}}$ by 2030, but can increase over India (up to 0.84 $\mathrm{W\,m^{-2}}$). The global values depend on the scenario and are lowest with the targeted SLCF simulation. The cloud radiative effect could decline 0.25–0.82 $\mathrm{W\,m^{-2}}$ by 2030 and occurs mostly over oceans, whereas the DRE effect is mostly over land. Our results show that targeted emission reduction measures can be a much better choice for the climate than overall high reductions globally. Our simulations also suggest that more than half of the near-future forcing change is due to the radiative effects associated with aerosol-cloud interactions.

1 Introduction

The net radiative forcing caused by atmospheric aerosol particles originating from human activities is currently negative, thereby offsetting a major, yet poorly-quantified fraction of the global warming caused by anthropogenic greenhouse gas emissions (Boucher et al., 2013; Smith and Mizrahi, 2013). The lifetime of atmospheric aerosol particles is relatively short, which has two major implications. Firstly, the climatically important aerosol properties vary greatly in both space and time in the atmosphere (e.g. Kaufman et al., 2002). Secondly, and perhaps even more importantly, atmospheric

ACPD
14, 31899–31942, 2014

Impacts of emission reductions on aerosol radiative effects

J.-P. Pietikäinen et al.

Title Page
Abstract | Introduction
Conclusions | References
Tables | Figures
◂◂ | ▸▸
◂ | ▸
Back | Close
Full Screen / Esc
Printer-friendly Version
Interactive Discussion

aerosol concentrations respond rapidly to any changes in emissions of either primary aerosol particles or aerosol precursor gases.

Overall increases in aerosol emissions during the past decades have contributed to the so-called global dimming, i.e. enhanced aerosol cooling effect, followed by some brightening due to later emission reductions in many regions of the world (e.g. Wild, 2009; Cermak et al., 2010; Haywood et al., 2011). In near future, there is a pressure for further aerosol and aerosol precursor emission reductions due to the adverse health effects by atmospheric aerosol particles (e.g. Pope and Dockery, 2006; Rao et al., 2012). This has raised concerns about loosing a significant fraction of the current aerosol cooling effect (Brasseur and Roeckner, 2005; Arneth et al., 2009; Raes and Seinfeld, 2009), and generated discussions on how to optimally realize future emission reductions (Löndahl et al., 2010; Shindell et al., 2012; Shoemaker et al., 2013; Smith and Mizrahi, 2013; Partanen et al., 2013).

The discussed mitigation strategies focus on reduction of black carbon (BC). While BC itself has an apparent warming effect in the present-day climate (e.g. Jacobson, 2010; Jones et al., 2011; Bond et al., 2013; Boucher et al., 2013), the usually co-emitted sulphur and organic compounds are effective cooling agents, substantially complicating the design of optimal emission reductions (Kopp and Mauzerall, 2010; Ramana et al., 2010). Furthermore, besides having a direct radiative effect on solar radiation, particles containing BC can act as cloud condensation and ice nuclei (Prenni et al., 2009; Leaitch et al., 2010). The influence of BC emission changes on clouds and climate is potentially important yet poorly quantified (Chen et al., 2010a; Bahadur et al., 2012; Bond et al., 2013).

The relation between future aerosol emission changes, radiative forcing and climate has been investigated both globally (Menon et al., 2008; Unger et al., 2009; Chen et al., 2010b; Bellouin et al., 2011; Makkonen et al., 2012; Gillett and Salzen, 2013; Levy et al., 2013; Smith and Bond, 2014) and over some continental regions (Mickley et al., 2012; Péré et al., 2012; Sillmann et al., 2013). While demonstrating potentially large regional effects, none of these studies have simultaneously considered the fol-

ACPD
14, 31899–31942, 2014

lowing issues together: the direct and indirect aerosol effects, the role of different world regions in these effects, and contrasting emission changes reflecting alternative emission control strategies. In this paper, we aim to bring new insight into these issues by investigating near-future changes in the aerosol direct and indirect radiative forcing globally as well as over a number of selected world regions as a result of emission changes according to four recently-developed emission scenarios. The specific questions, we are searching answers for are following:

- how much is the global negative aerosol forcing expected to be reduced during the next couple of decades from the present day value?
- how these changes differ over different world regions?
- what are the relative roles of direct and indirect effects?
- to what extent these patterns can be influenced by targeted emission reductions?

The paper is structured as follows: first, the model and the emission modifications are described in Sect. 2; Sect. 3 presents a detailed analysis of the results and explains the emission reductions influences to the climate, followed by Sect. 4, where the main conclusions are listed and further steps are discussed.

2 Methods

2.1 Model description

The main tool in this work is the global aerosol–climate model ECHAM-HAMMOZ (version ECHAM5.5-HAM2.0) (Zhang et al., 2012), which uses the HAM aerosol module (Stier et al., 2005) and the M7 aerosol microphysical module (Vignati et al., 2004). ECHAM-HAMMOZ simulates all the major aerosol sources (both natural and anthropogenic), microphysical processes and sinks. It predicts the evolution of seven interacting internally- and externally-mixed aerosol modes in terms of their size distribution

ACPD
14, 31899–31942, 2014

and composition. The simulated aerosol components are sulphate, BC, organic carbon (OC), sea salt and mineral dust. The aerosol module is coupled with the host model's stratiform cloud scheme and radiation module; thus, both the direct and indirect aerosol effects are simulated online (Lohmann and Hoose, 2009). The cloud droplet activation is calculated using a parametrization by Abdul-Razzak and Ghan (2000).

The aerosol characteristics simulated by ECHAM-HAMMOZ have been evaluated in several previous studies. For example, ECHAM-HAMMOZ was included in the Aero-Com model intercomparison exercise analyzing the life cycles of dust, sea salt, sulfate, black carbon and particulate organic matter in 16 global aerosol models (e.g Huneeus et al., 2011; Mann et al., 2014; Tsigaridis et al., 2014). Furthermore, Zhang et al. (2012) evaluated the ECHAM5-HAM2 version, which is used in this study, against the Aero-Com models and a large range of atmospheric measurements. These studies have shown that ECHAM-HAMMOZ can reproduce the main aerosol characteristics realistically. Thus in this study, we do not concentrate on model evaluation as such, although we do compare our simulated aerosol burdens and radiative effects to several previous model studies.

2.2 Emissions

For this work, some of the emission modules of ECHAM-HAMMOZ were updated and some new ones implemented. In the following sections, the modified and new modules are described in more detail. The global emissions maps for BC, OC and sulphur dioxide (SO_2) based on the new emissions are shown in the Supplement (Figs. S1–S3). Note that volcanic, dimethyl sulphide (DMS), dust and sea salt emissions are left unmodified and follow the methods presented in Stier et al. (2005) and Zhang et al. (2012).

ACPD
14, 31899–31942, 2014

2.2.1 Continental anthropogenic emissions

For anthropogenic emissions, we applied gridded datasets based on the GAINS (Greenhouse gas–Air pollution Interactions and Synergies) model (Amann et al., 2011), operated by the International Institute for Applied Systems Analysis (IIASA, http://gains.iiasa.ac.at). Globally, this model considers 162 geographical regions and includes all major economic sectors. The principal statistical data used in the model for the base year (2005) in our simulations (simulation Refe2005) originates from the International Energy Agency (IEA) and EUROSTAT, whereas for agriculture the data is from FAO (UN Food and Agriculture Organization).

In addition to the reference simulation, we considered four scenarios drawing on the energy projections presented in the World Energy Outlook 2009 (IEA, 2009) and including different assumptions of legislative and technological developments in the next few decades. The CLEC scenario includes all currently agreed air pollution policies and legislation and estimates impacts on emissions in 2020 and 2030 (simulations CLEC2020 and CLEC2030, respectively). The CLECC scenario includes these same policies, but is further designed to keep the total forcing due to long-lived greenhouse gases at 450 ppm CO_2-equivalent level by the end of the century via CO_2 mitigation measures mostly targeting the energy and industrial sectors (simulations CLECC2020 and CLECC2030) – this scenario relies on the 2° (450 ppm) energy scenario developed by IEA (IEA, 2009). In addition, two more scenarios for 2030 were used. The BCAdd scenario targets the short-lived climate forcers (SLCFs) by including a portfolio of most important measures that could yield the largest reductions in their global radiative forcing in 2030 (simulation BCadd2030). The principles of such scenario has been described in UNEP (2011) and Shindell et al. (2012). In terms of aerosols, this means targeting BC and OC emissions. Measures with a relatively small net impact or increase in radiative forcing have been excluded from this portfolio. Lastly, the MTFR scenario implements the maximum reduction potential of anthropogenic aerosol and SO_2 emissions with currently available technologies by year 2030 (simulation MTFR2030). The

ACPD
14, 31899–31942, 2014

MTFR scenario includes primarily end-of-pipe measures and excludes any further efficiency or fuel switching potential. For more detailed description of the current legislation and the MTFR scenarios see for example Cofala et al. (2007) and Klimont et al. (2009).

In this study, the GAINS detailed sectoral emissions were aggregated into six key categories: (1) agriculture (waste burning on fields), (2) residential and commercial combustion, (3) power plants, energy conversion, extraction, (4) industry (combustion and processing), (5) surface transportation and (6) waste. In addition, an extra sector for other SO_2 emissions not covered separately in GAINS was included. Each of the sectors are allocated into $0.5^\circ \times 0.5^\circ$ grid. The emissions from agriculture, residential and commercial combustion, surface transportation and waste sectors are emitted at the surface level. The energy sector emissions are released into following model levels: 51.25 % to 2nd lowest level, 45.3 % to 3rd lowest level and 3.45 % to 4th lowest level. The industrial sector and the extra sector for SO_2 emissions have the same vertical emission height distribution: 95 % to surface and 5 % to 2nd lowest level. The emission heights are based on Bieser et al. (2011).

By default, GAINS provides only the total annual emissions for all sectors. Considering the importance of temporal resolution for few key sectors, we have developed monthly estimates for power plants and residential combustion, and used GFED (see Sect. 2.2.3) temporal pattern for agricultural residue burning. Specifically for residential combustion we have applied the method developed by Streets et al. (2003), who calculated the operating hours for stoves based on monthly mean temperature, i.e., $< 0\,^\circ\mathrm{C} \Rightarrow 16\,\mathrm{h\,d^{-1}}$, 0–$5\,^\circ\mathrm{C} \Rightarrow 12\,\mathrm{h\,d^{-1}}$, 5–$10\,^\circ\mathrm{C} \Rightarrow 6\,\mathrm{h\,d^{-1}}$ and $> 10\,^\circ\mathrm{C} \Rightarrow 3\,\mathrm{h\,d^{-1}}$. In our approach, the monthly mean temperatures were obtained from the Climatic Research Unit (CRU) TS 3.1 dataset (Harris et al., 2013) and the calculations were done in each gridbox separately. Since our aim is to study the scenarios in current day climate conditions, the temperatures from 2005 were used for all GAINS emissions.

ACPD
14, 31899–31942, 2014

2.2.2 Aviation emissions

We also implemented into ECHAM-HAMMOZ the monthly aviation emission data produced in QUANTIFY (Quantifying the Climate Impact of Global and European Transport Systems) project (Lee et al., 2005; Owen et al., 2010). Concerning the aerosol species and precursors of interest in our work, only BC mass and number concentration are available (no data for OC or SO_2). The data is provided on a 1° resolution and at 23 levels using 610 m vertical steps. Since the QUANTIFY database provides emissions only for year 2000, we scaled the emission by 1.3355 in 2005, by 2.4 in 2020 and by 3.1 in 2030. These scaling factors were estimated based on Fig. 6 in Lee et al. (2010).

2.2.3 Wildfire emissions

The Global Fire Emissions Database (GFED) dataset for the wildfire emissions was updated to the version 3 (Giglio et al., 2010; van der Werf et al., 2010). The data has a 0.5° spatial resolution and is on a monthly time resolution. To make the emissions height dependent, the same approach as was used by Dentener et al. (2006) with AeroCom emissions was applied. GFED 3 dataset includes six different sectors: (1) deforestation and degradation fire emissions, (2) savanna fire emissions, (3) woodland fire emissions, (4) forest fire emissions, (5) agricultural waste burning, and (6) tropical peatland burning (confined to Indonesia and Malaysian Borneo) (van der Werf et al., 2010). The 5th sector can be also found in the GAINS model output (see Sect. 2.2.1) and in this work the GAINS agriculture sector was used. Moreover, for all simulated years, the 2005 GFED emissions were used.

2.2.4 Shipping emissions

The international ship emissions are based on the improved ICOADS (International Comprehensive Ocean–Atmosphere Data Set) data by Wang et al. (2008). In this work, the RCP 8.5 (Riahi et al., 2007) emission estimates for the years 2005, 2020 and 2030 were used. The sensitivity of the results to the chosen RCP was tested by repeating the reference simulation (Refe2005) using RCP 2.6 emissions. However, the difference between the two RCPs was found to be so small that no further analysis will be shown from RCP 2.6 simulations.

The annual global emissions from shipping according to RCP 8.5 are represented in Table 1. Since the ICOADS dataset presents only a proxy grid on a 0.1° horizontal resolution, i.e. the dataset gives the fraction of total global ship emissions that is emitted at each grid cell, final gridded emissions were obtained by using the global proxy with the values from Table 1. Since the proxy does not include estimates how the shipping routes will change in the future, the same emission pattern is used for all simulations.

In the Arctic, we have used an additional high resolution emission inventory by Corbett et al. (2010). In this inventory, the data is given on a seasonal scale in a 5 km × 5 km horizontal grid for year 2004, including 2020 and 2030 as scenario years. We used the emission values for 2004 in our reference simulation for year 2005 without any modifications; it can be assumed that the error from this approach lies within the uncertainty limits of the emissions. For the scenario years 2020 and 2030, the Business As Usual (BAU) approach was chosen. The scenarios also include changes in the shipping route patterns (details in Corbett et al., 2010). If there were overlapping grid boxes between ICOADS and Arctic emission datasets, the latter was chosen.

2.3 Simulations

Each simulation was run for 5 years (2003–2007) preceded by a 6 month spin-up. In order to minimize the variation in the model meteorology, all the simulations were nudged (i.e. divergence, vorticity, surface pressure and temperature were forced to follow) towards the ERA-Interim reanalysis data (Dee et al., 2011). The 5 year monthly data was furthermore averaged to one year monthly data (multi-year monthly mean), which minimizes the influence of the internal variability of the model. All simulations were conducted at a T63 horizontal resolution (∼ 200 km) with 31 vertical terrain following levels (top reaching 10 hPa).

ACPD
14, 31899–31942, 2014

We have also done shorter simulations where the aerosol characteristics were compared to simulations with original emissions (not shown here). Based on these simulations, the new version reproduces closely the aerosol fields of the original model version.

3 Results and discussion

Below, we concentrate mainly on the 2030 simulation results, and discuss year 2020 only when it reveals additional information about the time scale of the emission reductions. All the absolute and relative changes presented are calculated as the difference between the scenario and reference simulation (Refe2005) values. In addition to global results, we analyse the simulations separately for the 8 regions shown in Fig. 1, i.e. Western United States, Eastern United States, South America, Europe, Africa, India, Western China and Eastern China. The column burdens and aerosol radiative effects for these regions are summarized in Tables 2 and 3.

3.1 Aerosol burdens

3.1.1 BC burden

The annual mean BC column burden results are shown in Fig. 2. In all the simulations, the BC burden peaks in the Amazon region and central Africa (biomass burning areas), India (residential biomass burning area) and Eastern China (industrial area). In these peak areas, changes in BC burden are relatively modest in most of the scenarios apart from CLEC2030, which shows a 32 % increase over India, and BCAdd2030 and MTFR2030, which both show nearly 60 % decreases over Eastern China (Table 2). Over India, the increase comes mainly from the traffic sector, which approximately doubles in CLEC2030 and reflects estimated growing population. However, it is noteworthy that the domestic sector will still have the biggest emissions over India. The decrease over Eastern China in the two mitigation scenarios (BCAdd and MTFR) is primarily due to declining use of solid fuels (mostly coal) for cooking and heating in residential combustion sector. The high BC burden areas in the biomass burning regions of South America and Africa show negligible change in all the scenario runs since the GAINS scenarios do not predict reductions for this sector (and the wildfire emissions from GFED are the same for all simulated years).

Concerning regions with lower absolute BC burden values, all scenarios predict significant decreases by 2030 over Europe (−24 to −66 %, mainly from residential combustion and traffic sectors) and North America (−3 to −54 %, mainly traffic sector), although in CLECC2030 the burden slightly increases over Mexico and southern parts of USA (increment over Western US 8 %, caused by residential combustion sector). Furthermore, in CLEC and CLECC scenarios BC burden increases over Africa (9 and 5 %, respectively; from residential combustion sector) and Western China (28 and 15 %, respectively; from residential combustion, traffic and industrial sectors). In these scenarios, small increases are seen also in Southern Argentina, the west coast and southern parts of Africa, and the border area of Indonesia and Papua New Guinea. Due to atmospheric transport, the BC burden also increases over Antarctica as well as over most oceanic regions in the Southern Hemisphere. Although the absolute BC values in these regions are low, the increased burdens could lead to changes to the surface albedo over snowy and sea ice covered areas. However, since the albedo change due to BC deposition is not included in the current model version, further investigation concerning this effect is left for future studies.

The two more extreme scenarios, i.e. BCAdd and MTFR, show decreased BC burden over the whole globe (−26 and −27 %, respectively). The differences between the burdens in these two scenarios are quite modest also on regional scale (Table 2), which means that the targeted sectors (transport and especially residential combustion) in BCAdd include most of the reduction potential of BC, even when all technologically available measures are used (as in MTFR). The additional reductions in MTFR come from waste disposal and treatment, and agricultural waste burning. MTFR scenario as-

ACPD
14, 31899–31942, 2014

sumes that all activity in these sectors can be stopped and thus their emissions are set to zero.

Our reference simulation can be compared to previous model estimates of atmospheric aerosol burden. Schulz et al. (2006) reported results from a multi-model comparison for global BC, OA and SO_4 burdens. For models using AeroCom emissions (2000), the global ensemble mean for BC was 0.25 $mg\,m^{-2}$. For models models resorting to other emission inventories, the global ensemble mean was 0.37 $mg\,m^{-2}$ for BC. In addition, Bond et al. (2013) collected results from recent publications (some same as in Schulz et al., 2006, details in the papers) and calculated a mean burden of 0.26 $mg\,m^{-2}$. These results are in good agreement with our result (0.25 $mg\,m^{-2}$, Table 2) and show that the new emissions can reproduce the global BC burden realistically.

3.1.2 Organic aerosol burden

The absolute values of organic aerosol (OA) burden in the reference simulation (Fig. 3) are higher than for the BC burden (almost by a factor of 10), but overall the burden maps are very similar. This reflects the fact that these two compounds are often co-emitted from the same sources but organic emissions dominate in magnitude, especially in the residential combustion sector. The OA burdens differ less between the different scenarios and show overall much smaller relative changes from the reference run than the BC burdens (compare Figs. 2 and 3). The main reason for this is the significant contribution of natural sources to the overall OA emissions, which diminish the influence of anthropogenic emission changes.

CLEC2030 and CLECC2030 scenarios predict the largest changes in OA burden over Eastern China (−25 and −31 %, respectively), mainly from the residential combustion sector due to reduction of solid fuel use and effective decline of stove emissions. On the other hand, changes over India, Europe and North America are very small, in contrast to the BC burden changes. The differing behavior of BC and OA burdens over India can be explained by the traffic sector, which increases the BC emissions more strongly in the future. The opposite can be seen in Europe and North America, where the reductions in BC emissions in the traffic sector are quite high whereas the OC reductions are much more moderate. This is because the reduction for traffic sector are focused on diesel emissions, which for aerosol emissions are mainly BC.

In BCAdd simulation, the OA burden decreases globally and the highest reductions are over Europe (−25 %, mainly from residential combustion and traffic sectors), India (−50 %, mainly residential combustion sector), Western China (−47 %, residential combustion sector) and Eastern China (−53 %, residential combustion and energy sectors). The geographical pattern of change is similar in MTFR, although the decrement is higher; the highest reductions occur over China, Japan, India, Middle-East and Europe reaching a −21 % decrement globally (all sectors decrease, residential combustion sector having the biggest reductions). In these two scenarios, the pattern of OA burden change is again quite different from pattern of BC burden change (compare Figs. 2 and 3). OA burden change is much more significant over India due to a very large contribution from both stoves and agricultural burning, and these two sources have high share of OC. On the other hand, larger BC changes are seen over Europe and North America as there are less stoves with high OC and instead most mitigation will be in diesel controls with high BC share and some in the residential combustion sector. It is also noticeable that changes over the Southern Hemisphere are small in all the scenarios.

The values for global OA from Schulz et al. (2006) are also in good agreement with our results. Again, if only the models which used AeroCom based emissions are taken into account, the global mean is 1.32 $mg\,m^{-2}$. For the other models, Schulz et al. (2006) reported a mean of 2.40 $mg\,m^{-2}$. Our results show a global OA burden of 2.01 $mg\,m^{-2}$, which falls into the range of the values reported in Schulz et al. (2006). The relatively large uncertainties in simulating the global and regional organic burdens arise from poorly quantified primary emissions and secondary organic aerosol formation, together with uncertainties in the sufficient complexity of the OA parameterizations (Tsigaridis et al., 2014).

ACPD
14, 31899–31942, 2014

3.1.3 Sulphate burden

The absolute sulphate aerosol (SA) burden map in Fig. 4 differs from BC and OA maps, because the anthropogenic emission sources are more similar between BC and OC than compared with SO_2. For BC and OC, the biggest source is the residential combustion sector, whereas SO_2 is mainly emitted from the industrial and energy sectors.

Figure 4 shows that the highest absolute values of SA burden are over Eastern China, India, Middle-East, North Africa, Southern Europe and Eastern USA. The latitudinal dependence of the burden over the continents is explained by the amount of solar radiation, which is needed for oxidation of SO_2 to sulphate.

In Europe, it is well known that sulphate precursor (SO_2) emissions have decreased over the last 2–3 decades (Hamed et al., 2010, and references therein). The same decreasing trend is also visible in the current legislation based simulations, which have reductions from 26 (CLEC2030) to 35 % (CLECC2030) over Europe. In North America, the reductions in SA burden are even higher, especially over Eastern and Central parts of USA. CLEC2030 gives −33 % decrement over Western US and −40 % over Eastern US, whereas in CLECC2030 the values are −41 and −48 %, respectively. These significant decreases in both Europe and North America are mainly from the energy sector, although, the industrial sector has also reductions that influence the results.

Quite the opposite can be seen over India, where the burden values increase in all scenarios, except in MFTR. The increment is smallest in CLECC2030 scenario being 12 % and the highest in CLEC2030 scenario (62 %), although almost as high increase (58 %) is simulated in the BCAdd scenario. On the other hand, in MTFR scenario the SA burden decreases by 60 %. These features come from the industrial and energy sectors and mean that the SA burden over India could be controlled with technical measures, such as flue gas desulphurization. It is noteworthy that in BCAdd the change is not significant in areas outside India, South Africa, Europe and US.

The global sulphate aerosol burden was also reported by Schulz et al. (2006). For AeroCom emissions based model, the global mean burden is 2.12 $mg\,m^{-2}$ and for other

ACPD
14, 31899–31942, 2014

models 2.70 $g\,m^{-2}$. Our results are slightly lower being 1.85 $mg\,m^{-2}$. However, our result is well in range of the modelled results shown by Schulz et al. (2006) and as there are differences in sources and sinks (e.g. different emission years, deposition modules etc), we feel confident to say that our result shows a realistic global SA burden.

3.1.4 Aerosol burdens in 2020

In order to explore the timeline of the emission reductions, we will show next results from the current legislation scenarios for the changes between 2005 and 2020. Summary of the burden changes between these years is included in Table 2 and Fig. S4.

Regarding BC burden, the same general features which were visible in CLEC2030 simulation can also be seen in CLEC2020. While the changes from 2005 through 2020 to 2030 do not follow a linear path, the CLEC2020 shows overall the same global pattern as CLEC2030 (Fig. S4). Globally, the BC burden increases 2 % between 2005 and 2020, and 5 % between 2005 and 2030, indicating an accelerated BC emission rate in the 2020s mainly from the traffic sector. Regionally, the biggest contributors to the increased burden in the 2020s are India and Western China (Table 2). In both of these regions the relative BC burden change (from the reference year 2005) almost doubles between 2020 and 2030. On the other hand, there is a significant decrease in the BC burden in Eastern China after 2020 (burden change of −4 % between 2005 and 2020, and −15 % between 2005 and 2030). This is caused by the reductions in residential combustion and energy sectors, although it should be mentioned that traffic sector increases between 2020 and 2030 in Eastern China roughly as much as energy sector decreases.

In CLECC scenario, the global values of BC burden decrease slightly between 2005 and 2020 (−0.2 %) and increase between 2005 and 2030 by 1 %. The reason for this is the same as in the CLEC scenario, i.e. the traffic sector. The geographical patterns of BC burden change are quite similar for CLECC2020 and CLECC2030; however, there are some significant differences over North America. At the border area of Mexico and

ACPD
14, 31899–31942, 2014

USA, the BC burden change shows no clear signal by 2020, but there is an increase by 2030. This can be also seen from the Table 2, where over Western US BC burden is decreased by 13 % by 2020, but increases 8 % by 2030. The difference comes from the residential combustion sector, which is estimated to increase quite significantly by 2030. The reason for this is that in CLECC the underlying idea is to move from fossil fuels to bio fuels and residential burning, which happens mainly between 2020 and 2030. Another place with big difference in CLECC between 2020 and 2030 is Eastern China, where the decrement (with respect to 2005) increases from −9 to −25 % and comes from the reductions in residential combustion and energy sectors. Similarly as in CLEC, the reduction in the energy sector are roughly balanced out by the increased traffic sector.

The global OA burden changes are small in both scenarios. However, in the CLEC scenario the burden increases 1.0 % between years 2005 and 2020, and 0.9 % between years 2005 and 2030, indicating a slight reduction during the 2020s. On the other hand, a much stronger reduction after 2020 takes place in the CLECC scenario as the OA burden change is smaller than −0.05 % by 2020 and −1 % by 2030. Regionally, the biggest differences are over Eastern China and the Mexico–USA border. The decrement over Eastern China increases between 2020 and 2030 in CLEC from −10 to −25 % and in CLECC from −15 to −31 %, mainly coming from the residential combustion sector. Over the Mexico–US border, the scenarios show no signal by 2020, but by 2030 both have strong positive sign; over Western USA the burden change in CLEC is −2 % by 2020 and 4 % by 2030, and in CLECC −2 and 13 %, respectively. As explained above, this is caused by the increases in residential combustion sector. In other regions the changes are quite small and do not show significant changes in the pattern of OA burden.

In terms of global SA burden, most of the reductions take place already before 2020 in both scenarios, and in fact the CLEC scenario predicts an increase of SA in the 2020s (change from year 2005 burden is −9 % by 2020 and −5 % by 2030). This increase in burden happens mainly because of the increment over India (from 25 %

ACPD
14, 31899–31942, 2014

change in 2020 to 62 % change in 2030) and Western China (from 15 to 42 %) and is caused by higher industrial and energy sector emissions. At the same, Europe and the Americas experience very low emission reductions, or even slight emission increases, in the 2020s. In CLECC scenario, the decreasing global trend in the SA burden continues throughout the 2020s, although it slightly slows down: the change from 2005 burden is −12 % by 2020 and −18 % by 2030. This global decrease is mainly caused by the decreasing trend in energy sector emissions. In this scenario, all studied regions show decreasing SA burdens between 2020 and 2030, with the largest decrease taking place in E China (burden change of −10 % in 2020 and −33 % in 2030). Over the other regions, the reductions after 2020 are at most 6 percentage units.

3.2 Radiative effects

We will next investigate how the simulated changes in the aerosol burden translate into aerosol radiative effects. As the radiative effects presented in the following sections are mostly negative, i.e. they have a cooling effect, the difference plots represent the change in the cooling. This means, that if the cooling increases in a scenario, the difference will be negative (more negative minus less negative gives a negative value). Naturally, if cooling decreases, the values are positive. This should be kept in mind when the radiative effect plots are analysed. Additionally, the values given in the following sections refer to the top of the atmosphere.

3.2.1 Direct radiative effect

Aerosols scatter and absorb the incoming solar radiation and the sum of these is called the direct radiative effect (DRE). DRE allows us to study how the radiation budget is changing in different scenarios due to aerosols. Besides short wave radiation permutations, aerosols can also influence the long wave radiation through absorption and emissivity (especially large particles, for example dust). However, this is has a minor significance for the smaller anthropogenic aerosols (Ramanathan and Feng, 2009).

ACPD
14, 31899–31942, 2014

We have conducted tests to estimate the magnitude of the long wave component in our simulations and, based on the results, the impact was found to be insignificant. Thus, DRE in our analysis is only calculated for the short wave radiation. It should also be noted that the DRE values are clear-sky values, which means that they are calculated assuming zero cloud cover.

Figure 5 shows the annual mean DRE for the reference run and the difference plots for the scenarios. The reference run shows that overall, DRE is negative around the world (global mean $-3.94\,\mathrm{W\,m^{-2}}$). Previous studies show similar estimates, for example, Yu et al. (2006) presented a review of DRE estimates and concluded it to be $-4.9 \pm 0.7\,\mathrm{W\,m^{-2}}$ over land and $-5.5 \pm 0.2\,\mathrm{W\,m^{-2}}$ over oceans. Since many of the satellite measurements only give estimates over oceans, we have also calculated this value from our simulations and got $-4.68\,\mathrm{W\,m^{-2}}$ (globally). This can be compared with Zhao et al. (2008), who estimated an oceanic DRE of $-4.98 \pm 1.67\,\mathrm{W\,m^{-2}}$, and with Forster et al. (2007), who estimated from satellite remote sensing studies a value of $-5.4\,\mathrm{W\,m^{-2}}$ (with SD of 0.9) over the oceans. Therefore, our simulations seem to give realistic values and are in accord with previous studies.

In the reference simulation, the strongest cooling caused by DRE takes place over Atlantic ocean near the coast of East Africa; this is mainly because of the dust transport from Sahara. The overall aerosol burden is also high over the polluted areas, for example Eastern China where it leads to cooling of $-5.16\,\mathrm{W\,m^{-2}}$. Over Europe, India, Africa and Eastern US the values are quite close to the global mean, whereas in Western China and Western US only approximately half of it. Over smaller regions DRE can be also positive (Fig. 5). This happens when the underlying surface has high albedo and the aerosols above are absorbing. This occurs mainly over Sahara, Antarctica and Greenland. Seasonally, positive DRE could be simulated also over Arctic and other snow-covered regions. Note that DRE could be also positive if the absorbing aerosol are above clouds, but here we use only clear-sky values.

Consistent with reductions in aerosol emissions, all the scenario simulations predict a decreasing trend of DRE over Europe and North America. The decrease is predicted

ACPD
14, 31899–31942, 2014

to be 0.5–1.0 $W m^{-2}$ over Europe, 0.9–1.3 $W m^{-2}$ over Eastern US, and 0.5–0.8 $W m^{-2}$ over Western US. The smallest decreases are seen in the CLEC and CLECC scenarios, and the largest in the MTFR scenario. These changes are mainly caused by reductions in SO_2 emissions, which lead to lower aerosol concentrations and thus decrease the cooling effect. The main sector causing these reductions is the energy production and distribution sector, which has the highest reductions in CLECC and MTRF scenarios. These reductions are also visible over Eastern China, where BCAdd and CLEC scenarios show modest reduction in DRE cooling (0.07 and 0.29 $W m^{-2}$, respectively), but much higher values in CLECC and MTRF scenarios (1.18 and 2.38 $W m^{-2}$, respectively).

The simulated DRE changes over India show significant variation between the different scenarios. Our simulations predict that the cooling effect will increase in BCAdd and CLEC (−1.32 and −0.84 $W m^{-2}$, respectively), no significant changes will occur in CLECC, whereas in MTFR, the cooling effect will decrease (1.15 $W m^{-2}$). The reason for this behavior can be searched from the changes in aerosol component burdens (Figs. 2–4).

As was shown in Sect. 3.1.1, the BC burden increases in CLEC and CLECC scenarios and decreases in BCAdd and MTRF scenarios. Thus, it is obvious that the sign of DRE does not directly follow the changes of BC burden. In addition, the OA burden changes over India quite similarly than the BC burden, and besides the overall OA changes are small compared to the other two components. This indicates that the role of OA in driving the DRE sign over India is not significant. Meanwhile, SA burden shows significant increases in BCAdd and CLEC scenarios, is quite modest in CLECC and decreases in MTRF. Thus apart from CLECC, the SA burden changes can explain the signal of DRE over India. In CLECC simulation, the increased absorption coming from the increased BC burden eliminates the cooling entirely (absorption maps are in the Supplement; Fig. S5). This means that, based on our model simulation predictions, the sign of DRE change over India is a combination of a warming component for which the changes are mainly caused by the residential combustion sector, and a cooling

ACPD
14, 31899–31942, 2014

component for which the changes are mainly due to energy production and distribution sector.

It is not straightforward to compare the simulated DRE changes to previously published estimates due to different baseline and scenario years, and differences in emission scenarios between the studies. Unger et al. (2009) undertook sensitivity studies with NASA Goddard Institute for Space Studies (GISS) model for future DRE change using 1995 as reference year and 2050 as scenario year. The authors reported global net reduction of 0.179 $W m^{-2}$ between these years. Out of our scenario runs, CLEC shows slightly lower reductions from 2005 to 2030 (0.11 $W m^{-2}$), and a decreasing trend in the 2020s (change from 2005 to 2020 is 0.13 $W m^{-2}$). On the other hand, CLECC shows somewhat higher values (0.24 $W m^{-2}$) than Unger et al. (2009), and no sign of changing trend. The predicted DRE in BCAdd and MTFR are clearly lower and higher, respectively, than simulated in Unger et al. (2009). When comparing these two studies, it should be noted that some of the reductions assumed by Unger et al. (2009) may have happened already before 2005, which we use as the reference year.

Szopa et al. (2013) simulated with a global earth system model the present day climate and future climate based on different RCP scenarios. Based on Fig. 14 in their work, we calculated the global and European forcing change between years 2005 and 2030. Globally, the change is 0.0–0.125 $W m^{-2}$ (depending on the RCP scenario), whereas our simulations show 0.06–0.4 $W m^{-2}$ change (or 0.11–0.24 $W m^{-2}$ if only CLEC and CLECC is considered). In Europe, Szopa et al. (2013) estimates a DRE change of 0.3–0.7 $W m^{-2}$, whereas our simulations predict 0.51–0.95 $W m^{-2}$ change (0.54–0.7 $W m^{-2}$ for CLEC and CLECC). On the other hand, Smith and Bond (2014) used the Global Change Assessment Model (GCAM) to estimate the future forcing changes, and calculated a global DRE of 0.175 $W m^{-2}$ between 2005 and 2030. Overall, our estimates of DRE change are well in line with the previous studies, especially given that there are many differences between the models and simulation set-ups used.

Our simulations were limited to the coming few decades; however, there are earlier published estimates on how the aerosol effect will change by the end of the century.

ACPD
14, 31899–31942, 2014

Chen et al. (2010b) reported a reduction of 0.12 $W\,m^{-2}$ between 2010 and 2100 based on three different models. Bellouin et al. (2011) showed that for the time period of 2000–2090, HadGEM2-ES model gives 0.32 $W\,m^{-2}$ reduction without nitrate and 0.83 $W\,m^{-2}$ when nitrate is included. Based on Szopa et al. (2013), the change between 2005 and 2090 was estimated to be 0.15–0.26 $W\,m^{-2}$ and based on Smith and Bond (2014), the change between 2005 and 2100 was estimated to be 0.47 $W\,m^{-2}$. These examples give some estimates on how DRE changes might continue after 2030.

3.2.2 Cloud radiative effect

Cloud radiative effect (CRE) is also a sum of two components: the short wave and long wave cloud radiative effects. As the short wave radiative effect is more dominant, the following analysis only includes the short wave component and makes the CRE analysis more consistent with the DRE analysis. Therefore as with DRE, from this point forward we will use the abbreviation CRE only for the short wave component.

CRE is calculated based on the method proposed by Ghan (2013), which removes the effects of aerosol scattering and absorption. The double-moment cloud scheme used in this work takes into account cloud droplet activation (Sect. 2.1). Freshly emitted insoluble BC can act as ice nuclei and thus influence ice clouds directly, but in case of warm clouds, only soluble aerosols have potential to act as cloud condensation nuclei (CCN). BC is emitted as insoluble, but can in our model become hygroscopic through condensation of sulphuric acid and coagulation with soluble particles.

Figure 6 shows the simulated global distribution of CRE and the difference plots between the reference year and scenarios. The largest values of CRE are seen over oceans ($> 100\,W\,m^{-2}$), mostly in temperate latitudes. Several continental areas, e.g. over Europe, China, Central Africa, North America and South America, have also quite high CRE. Based on all the scenario simulations, the cooling from CRE will decrease in the future. This takes place mainly in the Northern Hemisphere where the change in CRE is over 2.5 $W\,m^{-2}$ in some areas. The reason for this is that most of the reductions

ACPD
14, 31899–31942, 2014

in emissions are located in the Northern Hemisphere. In all scenarios, CRE changes over North Atlantic Ocean, North Pacific Ocean and Europe. Furhermore, BCAdd2030 and MTFR2030 show decreases also over Eastern China and the coast of Peru, and MTFR2030 for example over East and West coasts of Africa and South coast of Brazil. Some minor changes also takes place in MTRF over the Southern Hemisphere, but the values are very low ($< 0.5\,\mathrm{W\,m^{-2}}$). It is noteworthy that globally the changes in the absolute values of CRE are approximately twice as large as the changes in the DRE (except for BCAdd, for which the CRE change is about six times as large as the DRE change). However, regionally, large variability in the relative magnitude of CRE and DRE can be seen.

The simulated reduction patterns in CRE follow approximately the reduction patterns of BC and SA burdens (Figs. 2 and 4). Over Northern Pacific Ocean and west coast of South America, BC burden seems to be a more dominant contributor to CRE, whereas over Atlantic Ocean and coastal areas of Africa, SA burden changes are the dominant factor. On the other hand, over India in the BCAdd scenario, increased SA burden does not lead to an increment in CRE values, because the influence is limited by reductions in BC.

Previously Szopa et al. (2013) estimated the indirect forcing to change between 2005 and 2030 by 0.05–0.1 $\mathrm{W\,m^{-2}}$. For the same time period, the estimate from Smith and Bond (2014) is 0.1 $\mathrm{W\,m^{-2}}$. These estimated values are less than half of our simulated CRE change (0.25–0.82 $\mathrm{W\,m^{-2}}$, Table 3). However, our model includes a sophisticated aerosol activation scheme that takes into account the aerosol number and composition size distribution, and simulates both first and second aerosol indirect effects. On the other hand, Szopa et al. (2013) include only the first aerosol indirect effect, and calculate the cloud droplet number concentration in a simplified way based on soluble aerosol mass. Smith and Bond (2014) do not utilize a global atmospheric model at all but obtain their CRE estimates via direct scaling of aerosol emissions. Therefore, these two previous studies are not directly comparable to our simulations.

ACPD
14, 31899–31942, 2014

It should be stressed that the approach here only tells how the clouds react to aerosol concentration changes in current climate conditions (we use year 2005 meteorology in all simulations). Furthermore, some error is introduced by the nudging method because it restricts some of the feedback processes. For example, if emission reductions change regional or global cloud features in a way that it should impact the overall circulation, these feedback processes will not be fully realized in our simulations. Nevertheless, our approach does show how clouds and their properties react to emission changes in current climatological conditions and gives indications on how the future cloud radiative effect might change.

3.2.3 Forcings in year 2020

Again, we investigate the timeline of changes in aerosol radiative effects by looking at the two simulations for year 2020 (CLEC2020 and CLECC2020). The results from these simulations are summarized in Table 3) and Fig. S6.

Our model results show that in CLEC the reduction of global cooling from DRE takes place prior to 2020; the cooling effect even slightly increases between 2020 and 2030 (change from 2005 is 0.13 $W m^{-2}$ by 2020 and 0.11 $W m^{-2}$ by 2030). On the other hand, in CLECC, the decrease in global direct aerosol cooling (i.e. warming) continues after the 2020s; the DRE change is 0.16 $W m^{-2}$ between 2005 and 2020 and 0.24 $W m^{-2}$ between 2005 and 2030. However, regional differences are large in both scenarios. For example, our model predicts that in the CLEC scenario the cooling trend will significantly accelerate between 2020 and 2030 in India and Western China. On the other hand, the warming trend accelerates in Eastern China over the same time period. In the CLECC scenario, Eastern and Western China experience 3 and 5 times larger DRE change, respectively, from 2005 to 2030 than from 2005 to 2020. Over India, the negative change in DRE in 2020 (i.e. cooling effect with respect to 2005) turns into a positive change by 2030 (i.e. warming effect).

CRE changes after 2020 show somewhat different behaviour in CLEC and CLECC scenarios. There is no further change in global CRE in CLEC in the 2020s, whereas in

ACPD
14, 31899–31942, 2014

Impacts of emission reductions on aerosol radiative effects

J.-P. Pietikäinen et al.

CLECC the CRE values continue decreasing changing from 0.29 $W m^{-2}$ (between 2005 and 2020) to 0.39 $W m^{-2}$ (between 2005 and 2030). The global change in CLECC from 2020 to 2030 is mainly caused by the change over Eastern China, where the change of CRE increases from 0.26 $W m^{-2}$ by 2020 to 0.75 $W m^{-2}$ by 2030. This is caused by overall reductions in all aerosol species. Otherwise, the changes after 2020 are rather small in both scenarios, which means that most of the emission reduction based CRE changes already takes place by 2020.

4 Summary and conclusions

We have used the global aerosol–climate model ECHAM-HAMMOZ to evaluate how the aerosol forcing is expected to decrease during the next couple of decades and how it can be influenced by emission reductions. This has been done by modifying the model to use new and updated emission modules. The biggest update was to include GAINS model anthropogenic emissions. With this version, four different emissions scenarios were investigated for year 2030, and the two of the scenarios where also run for 2020. Year 2005 was used as a reference year. The scenarios included two different current legislation scenarios (CLEC and CLECC), one targeted to black carbon emission reductions (BCAdd) and one introducing the maximum reduction potential of aerosols and SO_2 with currently available technologies (MTFR).

With the current legislation scenarios, the global black carbon (BC) aerosol burden was estimated to increase by 2030 compared with the current (2005) situation, the sulphate aerosol (SA) burden was estimated to decrease and the organic aerosol (OA) burden may change either way. In the same scenarios, the BC and OA burdens showed increase over India, Western China, Africa and South America and the SA burden showed increases over India and Western China. The residential combustion and traffic sectors cause the major changes for BC and OC, while energy and industrial sectors cause most of the SA changes. Over South America, increases in the agricultural waste burning explain the higher burden for BC and OA in 2030. The targeted and maximum

ACPD
14, 31899–31942, 2014

technological reductions show decreasing trend for all species globally and regionally, except over India and Western China. There, the BC targeted simulation increases the SA burden due to increases in industrial and energy sectors.

The magnitude of negative aerosol forcing will decrease on a global scale in all scenarios. Based on the current legislation scenarios, the cooling coming from the direct radiative effect (DRE), compared to the year 2005, will decrease by 0.11–0.24 $W m^{-2}$ by 2030. The technical maximum potential for DRE reductions is globally 0.4 $W m^{-2}$ by 2030. Regionally, the cooling effect of DRE can also increase, for example over India and Western China. These changes follow mainly the BC and SA concentrations, which have different signs when the impact to DRE is considered. SA, having higher concentration, is more dominant and causes cooling through scattering, while BC has the ability absorb solar radiation and causes heating. For example over India, the cooling from DRE was estimated to increase due to increases SA burden, although in one current legislation simulation the increased BC burden seems to have an extinctive effect.

The magnitude of the cloud radiative effect (CRE), will decrease globally by 0.25–0.82 $W m^{-2}$ by 2030 compared with year 2005. These changes and patterns are again connected to BC and SA burden changes. Major changes mostly happen already by 2020. Overall, CRE is more dominant globally than DRE and has bigger changes. On the other hand, regionally the changes in DRE can be bigger, for example over India and Western China. The changes in CRE occur mostly over oceans, whereas in terms of DRE, most influence is seen over the continents. Globally, the changes in DRE are roughly half of the changes in CRE in most scenarios, but regionally large variability in the relative change can be seen.

Regionally, the cooling effect from DRE and CRE will increase over India and Western China, whereas elsewhere the cooling effect decreases. This is because the aerosol burden increases over India and Western China, and decreases elsewhere. The residential combustion and traffic sector causes the major changes for BC and OC, while energy and industrial sector causes most of the SA changes.

ACPD
14, 31899–31942, 2014

Our simulations predict a notable positive radiative forcing, up to about 1 $W m^{-2}$ globally and > 5 $W m^{-2}$ regionally, due to the reductions in aerosol and their precursor gas emissions that will take place during the next couple of decades. The magnitude of this forcing depends strongly on the chosen emission pathway. We have shown that targeted BC emission reductions are clearly the most beneficial for climate, making it even possible to achieve further enhancements in the negative direct radiative forcing (i.e. cooling effect) in some of the world regions (e.g. India and West China). To the contrary, reducing aerosol and their precursor emissions as much as it is technically feasible could probably be harmful for climate practically in all continental regions, although potentially beneficial from human health protection point of view. Finally, our simulations suggest that more than half of the near-future forcing change is due to the radiative effects associated with aerosol-cloud interactions. Noting this and the large uncertainties associated with this phenomenon (Boucher et al., 2013), more work is clearly needed for investigating the sources of cloud active aerosol particles into the atmosphere, aerosol-cloud-precipitation interactions and associated feedbacks in the climate system.

The Supplement related to this article is available online at doi:10.5194/acpd-14-31899-2014-supplement.

Acknowledgements. This work was supported by the EU Life+ project (LIFE09 ENV/FI/000572 MACEB), the Academy of Finland Research Programme for Climate Change FICCA (project 140748) and the EU FP7 IP PEGASOS (FP7-ENV-2010/265148). Gridding of the GAINS emission data by Chris Heyes is gratefully acknowledged. The ECHAM-HAMMOZ model is developed by a consortium composed of ETH Zurich, Max Planck Institut für Meteorologie, Forschungszentrum Jülich, University of Oxford, and the Finnish Meteorological Institute and managed by the Center for Climate Systems Modeling (C2SM) at ETH Zurich.

References

Abdul-Razzak, H. and Ghan, S. J.: A parameterization of aerosol activation: 2. Multiple aerosol types, J. Geophys. Res.-Atmos., 105, 6837–6844, doi:10.1029/1999JD901161, 2000. 31903

Amann, M., Bertok, I., Borken-Kleefeld, J., Cofala, J., Heyes, C., Höglund-Isaksson, L., Klimont, Z., Nguyen, B., Posch, M., Rafaj, P., Sandler, R., Schöpp, W., Wagner, F., and Winiwarter, W.: Cost-effective control of air quality and greenhouse gases in Europe: modeling and policy applications, Environ. Modell. Softw., 26, 1489–1501, doi:10.1016/j.envsoft.2011.07.012, 2011. 31904

Arneth, A., Unger, N., Kulmala, M., and Andreae, M. O.: Clean the air, heat the planet?, Science, 326, 672–673, doi:10.1126/science.1181568, 2009. 31901

Bahadur, R., Russell, L. M., Jacobson, M. Z., Prather, K., Nenes, A., Adams, P., and Seinfeld, J. H.: Importance of composition and hygroscopicity of BC particles to the effect of BC mitigation on cloud properties: application to California conditions, J. Geophys. Res.-Atmos., 117, D09204, doi:10.1029/2011JD017265, 2012. 31901

Bellouin, N., Rae, J., Jones, A., Johnson, C., Haywood, J., and Boucher, O.: Aerosol forcing in the Climate Model Intercomparison Project (CMIP5) simulations by HadGEM2-ES and the role of ammonium nitrate, J. Geophys. Res.-Atmos., 116, D20206, doi:10.1029/2011JD016074, 2011. 31901, 31919

Bieser, J., Aulinger, A., Matthias, V., Quante, M., and van der Gon, H. D.: Vertical emission profiles for Europe based on plume rise calculations, Environ. Pollut., 159, 2935–2946, doi:10.1016/j.envpol.2011.04.030, 2011. 31905

Bond, T. C., Doherty, S. J., Fahey, D. W., Forster, P. M., Berntsen, T., DeAngelo, B. J., Flanner, M. G., Ghan, S., Kärcher, B., Koch, D., Kinne, S., Kondo, Y., Quinn, P. K., Sarofim, M. C., Schultz, M. G., Schulz, M., Venkataraman, C., Zhang, H., Zhang, S., Bellouin, N., Guttikunda, S. K., Hopke, P. K., Jacobson, M. Z., Kaiser, J. W., Klimont, Z., Lohmann, U., Schwarz, J. P., Shindell, D., Storelvmo, T., Warren, S. G., and Zender, C. S.: Bounding the role of black carbon in the climate system: a scientific assessment, J. Geophys. Res.-Atmos., 118, 5380–5552, doi:10.1002/jgrd.50171, 2013. 31901, 31910

Boucher, O., Randall, D., Artaxo, P., Bretherton, C., Feingold, G., Forster, P., Kerminen, V.-M., Kondo, Y., Liao, H., Lohmann, U., Rasch, P., Satheesh, S., Sherwood, S. B. S., and Zhang, X.: Clouds and aerosols, in: Climate Change 2013: The Physical Science Basis. Contribution of Working Group I to the Fifth Assessment Report of the Intergovernmental Panel on Climate Change, edited by: Stocker, T. F., Qin, D., Plattner, G.-K., Tignor, M., Allen, S. K., Boschung, J., Nauels, A., Xia, Y., Bex, V., and Midgley, P. M., Cambridge University Press, Cambridge, UK and New York, NY, USA, doi:10.1017/CBO9781107415324.016, 571–658, 2013. 31900, 31901, 31924

Brasseur, G. P. and Roeckner, E.: Impact of improved air quality on the future evolution of climate, Geophys. Res. Lett., 32, L23704, doi:10.1029/2005GL023902, 2005. 31901

Cermak, J., Wild, M., Knutti, R., Mishchenko, M. I., and Heidinger, A. K.: Consistency of global satellite-derived aerosol and cloud data sets with recent brightening observations, Geophys. Res. Lett., 37, L21704, doi:10.1029/2010GL044632, 2010. 31901

Chen, W.-T., Lee, Y. H., Adams, P. J., Nenes, A., and Seinfeld, J. H.: Will black carbon mitigation dampen aerosol indirect forcing?, Geophys. Res. Lett., 37, L09801, doi:10.1029/2010GL042886, 2010a. 31901

Chen, W.-T., Nenes, A., Liao, H., Adams, P. J., Li, J.-L. F., and Seinfeld, J. H.: Global climate response to anthropogenic aerosol indirect effects: present day and year 2100, J. Geophys. Res.-Atmos., 115, D12207, doi:10.1029/2008JD011619, 2010b. 31901, 31919

Cofala, J., Amann, M., Klimont, Z., Kupiainen, K., and Höglund-Isaksson, L.: Scenarios of global anthropogenic emissions of air pollutants and methane until 2030, Atmos. Environ., 41, 8486–8499, doi:10.1016/j.atmosenv.2007.07.010, 2007. 31905

Corbett, J. J., Lack, D. A., Winebrake, J. J., Harder, S., Silberman, J. A., and Gold, M.: Arctic shipping emissions inventories and future scenarios, Atmos. Chem. Phys., 10, 9689–9704, doi:10.5194/acp-10-9689-2010, 2010. 31907

Dee, D. P., Uppala, S. M., Simmons, A. J., Berrisford, P., Poli, P., Kobayashi, S., Andrae, U., Balmaseda, M. A., Balsamo, G., Bauer, P., Bechtold, P., Beljaars, A. C. M., van de Berg, L., Bidlot, J., Bormann, N., Delsol, C., Dragani, R., Fuentes, M., Geer, A. J., Haimberger, L., Healy, S. B., Hersbach, H., Hólm, E. V., Isaksen, L., Kållberg, P., Köhler, M., Matricardi, M., McNally, A. P., Monge-Sanz, B. M., Morcrette, J.-J., Park, B.-K., Peubey, C., de Rosnay, P., Tavolato, C., Thépaut, J.-N., and Vitart, F.: The ERA-Interim reanalysis: configuration and performance of the data assimilation system, Q. J. Roy. Meteor. Soc., 137, 553–597, doi:10.1002/qj.828, 2011. 31907

Dentener, F., Kinne, S., Bond, T., Boucher, O., Cofala, J., Generoso, S., Ginoux, P., Gong, S., Hoelzemann, J. J., Ito, A., Marelli, L., Penner, J. E., Putaud, J.-P., Textor, C., Schulz, M., van der Werf, G. R., and Wilson, J.: Emissions of primary aerosol and precursor gases in the years 2000 and 1750 prescribed data-sets for AeroCom, Atmos. Chem. Phys., 6, 4321–4344, doi:10.5194/acp-6-4321-2006, 2006. 31906

Forster, P., Ramaswamy, V., Artaxo, P., Berntsen, T., Betts, R., Fahey, D., Haywood, J., Lean, J., Lowe, D., Myhre, G., Nganga, J., Prinn, R., Raga, G., Schulz, M., and Dorland, R. V.: Changes in atmospheric constituents and in radiative forcing, in: Climate Change 2007: The Physical Science Basis. Contribution of Working Group I to the Fourth Assessment Report of the Intergovernmental Panel on Climate Change, edited by: Solomon, S., Qin, D., Manning, M., Chen, Z., Marquis, M., Averyt, K. B., Tignor, M., and Miller, H. L., Cambridge University Press, Cambridge, UK and New York, NY, USA, 2007. 31916

Ghan, S. J.: Technical Note: Estimating aerosol effects on cloud radiative forcing, Atmos. Chem. Phys., 13, 9971–9974, doi:10.5194/acp-13-9971-2013, 2013. 31919

Giglio, L., Randerson, J. T., van der Werf, G. R., Kasibhatla, P. S., Collatz, G. J., Morton, D. C., and DeFries, R. S.: Assessing variability and long-term trends in burned area by merging multiple satellite fire products, Biogeosciences, 7, 1171–1186, doi:10.5194/bg-7-1171-2010, 2010. 31906

Gillett, N. P. and Salzen, K. V.: The role of reduced aerosol precursor emissions in driving near-term warming, Environ. Res. Lett., 8, 034008, doi:10.1088/1748-9326/8/3/034008, 2013. 31901

Hamed, A., Birmili, W., Joutsensaari, J., Mikkonen, S., Asmi, A., Wehner, B., Spindler, G., Jaatinen, A., Wiedensohler, A., Korhonen, H., Lehtinen, K. E. J., and Laaksonen, A.: Changes in the production rate of secondary aerosol particles in Central Europe in view of decreasing SO_2 emissions between 1996 and 2006, Atmos. Chem. Phys., 10, 1071–1091, doi:10.5194/acp-10-1071-2010, 2010. 31912

Harris, I., Jones, P., Osborn, T., and Lister, D.: Updated high-resolution grids of monthly climatic observations – the CRU TS3.10 Dataset, Int. J. Climatol., 34, 623–642, doi:10.1002/joc.3711, 2013. 31905

Haywood, J. M., Bellouin, N., Jones, A., Boucher, O., Wild, M., and Shine, K. P.: The roles of aerosol, water vapor and cloud in future global dimming/brightening, J. Geophys. Res.-Atmos., 116, D20203, doi:10.1029/2011JD016000, 2011. 31901

Huneeus, N., Schulz, M., Balkanski, Y., Griesfeller, J., Prospero, J., Kinne, S., Bauer, S., Boucher, O., Chin, M., Dentener, F., Diehl, T., Easter, R., Fillmore, D., Ghan, S., Ginoux, P., Grini, A., Horowitz, L., Koch, D., Krol, M. C., Landing, W., Liu, X., Mahowald, N., Miller, R., Morcrette, J.-J., Myhre, G., Penner, J., Perlwitz, J., Stier, P., Takemura, T., and Zender, C. S.:

ACPD

14, 31899–31942, 2014

Impacts of emission reductions on aerosol radiative effects

J.-P. Pietikäinen et al.

Global dust model intercomparison in AeroCom phase I, Atmos. Chem. Phys., 11, 7781–7816, doi:10.5194/acp-11-7781-2011, 2011. 31903

IEA: World Energy Outlook 2009, OECD Publishing, Paris, 650 pp., 2009. 31904

Jacobson, M. Z.: Short-term effects of controlling fossil-fuel soot, biofuel soot and gases, and methane on climate, Arctic ice, and air pollution health, J. Geophys. Res.-Atmos., 115, D14209, doi:10.1029/2009JD013795, 2010. 31901

Jones, G. S., Christidis, N., and Stott, P. A.: Detecting the influence of fossil fuel and bio-fuel black carbon aerosols on near surface temperature changes, Atmos. Chem. Phys., 11, 799–816, doi:10.5194/acp-11-799-2011, 2011. 31901

Kaufman, Y. J., Tanre, D., and Boucher, O.: A satellite view of aerosols in the climate system, Nature, 419, 215–223, 2002. 31900

Klimont, Z., Cofala, J., Xing, J., Wei, W., Zhang, C., Wang, S., Kejun, J., Bhandari, P., Mathur, R., Purohit, P., Rafaj, P., Chambers, A., Amann, M., and Hao, J.: Projections of SO_2, NO_x and carbonaceous aerosols emissions in Asia, Tellus B, 61, 602–617, 2009. 31905

Kopp, R. E. and Mauzerall, D. L.: Assessing the climatic benefits of black carbon mitigation, P. Natl. Acad. Sci. USA, 107, 11703–11708, doi:10.1073/pnas.0909605107, 2010. 31901

Leaitch, W. R., Lohmann, U., Russell, L. M., Garrett, T., Shantz, N. C., Toom-Sauntry, D., Strapp, J. W., Hayden, K. L., Marshall, J., Wolde, M., Worsnop, D. R., and Jayne, J. T.: Cloud albedo increase from carbonaceous aerosol, Atmos. Chem. Phys., 10, 7669–7684, doi:10.5194/acp-10-7669-2010, 2010. 31901

Lee, D., Pitari, G., Grewe, V., Gierens, K., Penner, J., Petzold, A., Prather, M., Schumann, U., Bais, A., Berntsen, T., Iachetti, D., Lim, L., and Sausen, R.: Transport impacts on atmosphere and climate: aviation, Atmos. Environ., 44, 4678–4734, doi:10.1016/j.atmosenv.2009.06.005, 2010. 31906

Lee, D. S., Owen, B., Graham, A., Fichter, C., Lim, L. L., and Dimitriu, D.: Allocation of International Aviation Emissions from Scheduled Air Traffic – Present Day and Historical (Report 2 of 3), Manchester Metropolitan University, Centre for Air Transport and the Environment, Manchester, UK, 2005. 31906

Levy, H., Horowitz, L. W., Schwarzkopf, M. D., Ming, Y., Golaz, J.-C., Naik, V., and Ramaswamy, V.: The roles of aerosol direct and indirect effects in past and future climate change, J. Geophys. Res.-Atmos., 118, 4521–4532, doi:10.1002/jgrd.50192, 2013. 31901

Lohmann, U. and Hoose, C.: Sensitivity studies of different aerosol indirect effects in mixed-phase clouds, Atmos. Chem. Phys., 9, 8917–8934, doi:10.5194/acp-9-8917-2009, 2009. 31903

Löndahl, J., Swietlicki, E., Lindgren, E., and Loft, S.: Aerosol exposure versus aerosol cooling of climate: what is the optimal emission reduction strategy for human health?, Atmos. Chem. Phys., 10, 9441–9449, doi:10.5194/acp-10-9441-2010, 2010. 31901

Makkonen, R., Asmi, A., Kerminen, V.-M., Boy, M., Arneth, A., Hari, P., and Kulmala, M.: Air pollution control and decreasing new particle formation lead to strong climate warming, Atmos. Chem. Phys., 12, 1515–1524, doi:10.5194/acp-12-1515-2012, 2012. 31901

Mann, G. W., Carslaw, K. S., Reddington, C. L., Pringle, K. J., Schulz, M., Asmi, A., Spracklen, D. V., Ridley, D. A., Woodhouse, M. T., Lee, L. A., Zhang, K., Ghan, S. J., Easter, R. C., Liu, X., Stier, P., Lee, Y. H., Adams, P. J., Tost, H., Lelieveld, J., Bauer, S. E., Tsigaridis, K., van Noije, T. P. C., Strunk, A., Vignati, E., Bellouin, N., Dalvi, M., Johnson, C. E., Bergman, T., Kokkola, H., von Salzen, K., Yu, F., Luo, G., Petzold, A., Heintzenberg, J., Clarke, A., Ogren, J. A., Gras, J., Baltensperger, U., Kaminski, U., Jennings, S. G., O'Dowd, C. D., Harrison, R. M., Beddows, D. C. S., Kulmala, M., Viisanen, Y., Ulevicius, V., Mihalopoulos, N., Zdimal, V., Fiebig, M., Hansson, H.-C., Swietlicki, E., and Henzing, J. S.: Intercomparison and evaluation of global aerosol microphysical properties among AeroCom models of a range of complexity, Atmos. Chem. Phys., 14, 4679–4713, doi:10.5194/acp-14-4679-2014, 2014. 31903

Menon, S., Unger, N., Koch, D., Francis, J., Garrett, T., Sednev, I., Shindell, D., and Streets, D.: Aerosol climate effects and air quality impacts from 1980 to 2030, Environ. Res. Lett., 3, 024004, doi:10.1088/1748-9326/3/2/024004, 2008. 31901

Mickley, L., Leibensperger, E., Jacob, D., and Rind, D.: Regional warming from aerosol removal over the United States: results from a transient 2010–2050 climate simulation, Atmos. Environ., 46, 545–553, doi:10.1016/j.atmosenv.2011.07.030, 2012. 31901

Owen, B., Lee, D. S., and Lim, L. L.: Flying into the future: aviation emissions scenarios to 2050, J. Am. Chem. Soc., 44, 2255–2260, doi:10.1021/es902530z, 2010. 31906

Partanen, A. I., Laakso, A., Schmidt, A., Kokkola, H., Kuokkanen, T., Pietikäinen, J.-P., Kerminen, V.-M., Lehtinen, K. E. J., Laakso, L., and Korhonen, H.: Climate and air quality trade-offs in altering ship fuel sulfur content, Atmos. Chem. Phys., 13, 12059–12071, doi:10.5194/acp-13-12059-2013, 2013. 31901

ACPD

14, 31899–31942, 2014

Péré, J., Colette, A., Dubuisson, P., Bessagnet, B., Mallet, M., and Pont, V.: Impacts of future air pollution mitigation strategies on the aerosol direct radiative forcing over Europe, Atmos. Environ., 62, 451–460, doi:10.1016/j.atmosenv.2012.08.046, 2012. 31901

Pope, C. A. and Dockery, D. W.: Health effects of fine particulate air pollution: lines that connect, J. Air Waste Manage., 56, 709–742, 2006. 31901

Prenni, A. J., Petters, M. D., Kreidenweis, S. M., Heald, C. L., Martin, S. T., Artaxo, P., Garland, R. M., Wollny, A. G., and Pöschl, U.: Relative roles of biogenic emissions and Saharan dust as ice nuclei in the Amazon basin, Nat. Geosci., 2, 402–405, 2009. 31901

Raes, F. and Seinfeld, J. H.: New directions: climate change and air pollution abatement: a bumpy road, Atmos. Environ., 43, 5132–5133, 2009. 31901

Ramana, M. V., Ramanathan, V., Feng, Y., Yoon, S.-C., Kim, S.-W., Carmichael, G. R., and Schauer, J. J.: Warming influenced by the ratio of black carbon to sulphate and the black-carbon source, Nat. Geosci., 3, 542–545, 2010. 31901

Ramanathan, V. and Feng, Y.: Air pollution, greenhouse gases and climate change: global and regional perspectives, Atmos. Environ., 43, 37–50, doi:10.1016/j.atmosenv.2008.09.063, 2009. 31915

Rao, S., Chirkov, V., Dentener, F., Van Dingenen, R., Pachauri, S., Purohit, P., Amann, M., Heyes, C., Kinney, P., Kolp, P., Klimont, Z., Riahi, K., and Schoepp, W.: Environmental modeling and methods for estimation of the global health impacts of air pollution, Environ. Model. Assess., 17, 613–622, doi:10.1007/s10666-012-9317-3, 2012. 31901

Riahi, K., Gruebler, A., and Nakicenovic, N.: Scenarios of long-term socio-economic and environmental development under climate stabilization, Technol. Forecast. Soc., 74, 887–935, doi:10.1016/j.techfore.2006.05.026, 2007. 31906

Schulz, M., Textor, C., Kinne, S., Balkanski, Y., Bauer, S., Berntsen, T., Berglen, T., Boucher, O., Dentener, F., Guibert, S., Isaksen, I. S. A., Iversen, T., Koch, D., Kirkevåg, A., Liu, X., Montanaro, V., Myhre, G., Penner, J. E., Pitari, G., Reddy, S., Seland, Ø., Stier, P., and Takemura, T.: Radiative forcing by aerosols as derived from the AeroCom present-day and pre-industrial simulations, Atmos. Chem. Phys., 6, 5225–5246, doi:10.5194/acp-6-5225-2006, 2006. 31910, 31911, 31912, 31913

Shindell, D., Kuylenstierna, J. C. I., Vignati, E., van Dingenen, R., Amann, M., Klimont, Z., Anenberg, S. C., Muller, N., Janssens-Maenhout, G., Raes, F., Schwartz, J., Faluvegi, G., Pozzoli, L., Kupiainen, K., Höglund-Isaksson, L., Emberson, L., Streets, D., Ramanathan, V., Hicks, K., Oanh, N. T. K., Milly, G., Williams, M., Demkine, V., and Fowler, D.: Simultaneously

ACPD

14, 31899–31942, 2014

Impacts of emission reductions on aerosol radiative effects

J.-P. Pietikäinen et al.

mitigating near-term climate change and improving human health and food security, Science, 335, 183–189, doi:10.1126/science.1210026, 2012. 31901, 31904

Shoemaker, J. K., Schrag, D. P., Molina, M. J., and Ramanathan, V.: What role for short-lived climate pollutants in mitigation policy?, Science, 342, 1323–1324, doi:10.1126/science.1240162, 2013. 31901

Sillmann, J., Pozzoli, L., Vignati, E., Kloster, S., and Feichter, J.: Aerosol effect on climate extremes in Europe under different future scenarios, Geophys. Res. Lett., 40, 2290–2295, doi:10.1002/grl.50459, 2013. 31901

Smith, S. J. and Bond, T. C.: Two hundred fifty years of aerosols and climate: the end of the age of aerosols, Atmos. Chem. Phys., 14, 537–549, doi:10.5194/acp-14-537-2014, 2014. 31901, 31918, 31919, 31920

Smith, S. J. and Mizrahi, A.: Near-term climate mitigation by short-lived forcers, P. Natl. Acad. Sci. USA, 110, 14202–14206, doi:10.1073/pnas.1308470110, 2013. 31900, 31901

Stier, P., Feichter, J., Kinne, S., Kloster, S., Vignati, E., Wilson, J., Ganzeveld, L., Tegen, I., Werner, M., Balkanski, Y., Schulz, M., Boucher, O., Minikin, A., and Petzold, A.: The aerosol–climate model ECHAM5-HAM, Atmos. Chem. Phys., 5, 1125–1156, doi:10.5194/acp-5-1125-2005, 2005. 31902, 31903

Streets, D. G., Bond, T. C., Carmichael, G. R., Fernandes, S. D., Fu, Q., He, D., Klimont, Z., Nelson, S. M., Tsai, N. Y., Wang, M. Q., Woo, J.-H., and Yarber, K. F.: An inventory of gaseous and primary aerosol emissions in Asia in the year 2000, J. Geophys. Res.-Atmos., 108, 8809, doi:10.1029/2002JD003093, 2003. 31905

Szopa, S., Balkanski, Y., Schulz, M., Bekki, S., Cugnet, D., Fortems-Cheiney, A., Turquety, S., Cozic, A., Déandreis, C., Hauglustaine, D., Idelkadi, A., Lathière, J., Lefevre, F., Marchand, M., Vuolo, R., Yan, N., and Dufresne, J.-L.: Aerosol and ozone changes as forcing for climate evolution between 1850 and 2100, Clim. Dynam., 40, 2223–2250, doi:10.1007/s00382-012-1408-y, 2013. 31918, 31919, 31920

Tsigaridis, K., Daskalakis, N., Kanakidou, M., Adams, P. J., Artaxo, P., Bahadur, R., Balkanski, Y., Bauer, S. E., Bellouin, N., Benedetti, A., Bergman, T., Berntsen, T. K., Beukes, J. P., Bian, H., Carslaw, K. S., Chin, M., Curci, G., Diehl, T., Easter, R. C., Ghan, S. J., Gong, S. L., Hodzic, A., Hoyle, C. R., Iversen, T., Jathar, S., Jimenez, J. L., Kaiser, J. W., Kirkevåg, A., Koch, D., Kokkola, H., Lee, Y. H, Lin, G., Liu, X., Luo, G., Ma, X., Mann, G. W., Mihalopoulos, N., Morcrette, J.-J., Müller, J.-F., Myhre, G., Myriokefalitakis, S., Ng, N. L., O'Donnell, D., Penner, J. E., Pozzoli, L., Pringle, K. J., Russell, L. M., Schulz, M., Sciare, J., Seland, Ø., Shindell, D. T., Sillman, S., Skeie, R. B., Spracklen, D., Stavrakou, T., Steenrod, S. D., Takemura, T., Tiitta, P., Tilmes, S., Tost, H., van Noije, T., van Zyl, P. G., von Salzen, K., Yu, F., Wang, Z., Wang, Z., Zaveri, R. A., Zhang, H., Zhang, K., Zhang, Q., and Zhang, X.: The AeroCom evaluation and intercomparison of organic aerosol in global models, Atmos. Chem. Phys., 14, 10845–10895, doi:10.5194/acp-14-10845-2014, 2014. 31903, 31911

UNEP: Near-Term Climate Protection and Clean Air Benefits: Actions for Controlling Short-Lived Climate Forcers, United Nations Environment Programme (UNEP), Nairobi, Kenya, 78 pp., 2011. 31904

Unger, N., Menon, S., Koch, D. M., and Shindell, D. T.: Impacts of aerosol-cloud interactions on past and future changes in tropospheric composition, Atmos. Chem. Phys., 9, 4115–4129, doi:10.5194/acp-9-4115-2009, 2009. 31901, 31918

van der Werf, G. R., Randerson, J. T., Giglio, L., Collatz, G. J., Mu, M., Kasibhatla, P. S., Morton, D. C., DeFries, R. S., Jin, Y., and van Leeuwen, T. T.: Global fire emissions and the contribution of deforestation, savanna, forest, agricultural, and peat fires (1997–2009), Atmos. Chem. Phys., 10, 11707–11735, doi:10.5194/acp-10-11707-2010, 2010. 31906

Vignati, E., Wilson, J., and Stier, P.: M7: an efficient size-resolved aerosol microphysics module for large-scale aerosol transport models, J. Geophys. Res.-Atmos., 109, D22202, doi:10.1029/2003JD004485, 2004. 31902

Wang, C., Corbett, J. J., and Firestone, J.: Improving spatial representation of global ship emissions inventories, Environ. Sci. Technol., 42, 193–199, doi:10.1021/es0700799, 2008. 31906

Wild, M.: Global dimming and brightening: a review, J. Geophys. Res.-Atmos., 114, D00D16, doi:10.1029/2008JD011470, 2009. 31901

Yu, H., Kaufman, Y. J., Chin, M., Feingold, G., Remer, L. A., Anderson, T. L., Balkanski, Y., Bellouin, N., Boucher, O., Christopher, S., DeCola, P., Kahn, R., Koch, D., Loeb, N., Reddy, M. S., Schulz, M., Takemura, T., and Zhou, M.: A review of measurement-based assessments of the aerosol direct radiative effect and forcing, Atmos. Chem. Phys., 6, 613–666, doi:10.5194/acp-6-613-2006, 2006. 31916

Zhang, K., O'Donnell, D., Kazil, J., Stier, P., Kinne, S., Lohmann, U., Ferrachat, S., Croft, B., Quaas, J., Wan, H., Rast, S., and Feichter, J.: The global aerosol–climate model ECHAM-HAM, version 2: sensitivity to improvements in process representations, Atmos. Chem. Phys., 12, 8911–8949, doi:10.5194/acp-12-8911-2012, 2012. 31902, 31903

ACPD

14, 31899–31942, 2014

Zhao, T. X.-P., Yu, H., Laszlo, I., Chin, M., and Conant, W. C.: Derivation of component aerosol direct radiative forcing at the top of atmosphere for clear-sky oceans, J. Quant. Spectrosc. Ra., 109, 1162–1186, doi:10.1016/j.jqsrt.2007.10.006, 2008. 31916

ACPD
14, 31899–31942, 2014

Impacts of emission reductions on aerosol radiative effects

J.-P. Pietikäinen et al.

Table 1. Yearly emissions fluxes for SO_2, BC and OC. Values are based on the RCP 8.5 estimates.

Year	SO_2 [$Tg\,a^{-1}$]	BC [$Tg\,a^{-1}$]	OC [$Tg\,a^{-1}$]
2005	13.050	0.141	0.150
2020	6.655	0.162	0.172
2030	6.328	0.170	0.181

ACPD
14, 31899–31942, 2014

Table 2. The areal mean burdens for the reference simulation and for the difference between the scenarios and the reference simulation.

	Globe	EU	India	Western China	Eastern China	Africa	Eastern United States	Western United States	South America
BC burden									
Refe2005 [mg m^{-2}]	0.25	0.26	1.20	0.72	1.03	0.72	0.20	0.17	0.34
CLEC2020 Δ[%]	2.2	−27.5	17.0	14.6	−4.4	5.1	−22.8	−15.3	0.7
CLEC2030 Δ[%]	5.0	−30.3	31.9	28.4	−15.0	8.9	−23.1	−10.2	2.0
CLECC2020 Δ[%]	−0.2	−27.5	10.9	8.7	−9.0	2.9	−17.7	−13.5	0.2
CLECC2030 Δ[%]	0.9	−24.1	17.9	15.0	−24.6	4.7	−3.1	8.4	1.2
BCAdd2030 Δ[%]	−25.8	−63.5	−30.7	−33.2	−58.6	−13.5	−47.2	−40.5	−9.5
MTFR2030 Δ[%]	−27.1	−66.3	−35.8	−37.9	−58.2	−13.7	−54.5	−48.3	−12.6
OA burden									
Refe2005 [mg m^{-2}]	2.01	1.02	6.25	3.87	4.54	6.34	1.67	1.51	4.59
CLEC2020 Δ[%]	1.0	−6.3	5.3	4.8	−10.4	3.1	−3.1	−1.9	0.1
CLEC2030 Δ[%]	0.9	−7.4	6.1	5.5	−24.9	4.4	−3.8	4.3	0.5
CLECC2020 Δ[%]	−0.0	−6.1	0.4	0.2	−14.6	2.1	−2.0	−2.1	0.3
CLECC2030 Δ[%]	−1.1	−4.7	−3.7	−3.7	−30.7	2.3	−0.0	12.6	0.5
BCAdd2030 Δ[%]	−16.5	−25.1	−49.7	−47.1	−53.5	−11.9	−12.4	−13.2	−3.7
MTFR2030 Δ[%]	−21.0	−34.1	−63.1	−60.9	−64.8	−15.2	−18.8	−20.2	−5.3
SA burden									
Refe2005 [mg m^{-2}]	1.85	2.37	4.35	2.73	5.31	2.88	2.98	2.60	1.54
CLEC2020 Δ[%]	−8.7	−27.6	25.1	14.6	−1.1	−13.2	−38.8	−31.5	−4.9
CLEC2030 Δ[%]	−5.1	−26.0	62.2	42.1	−6.9	−9.5	−40.1	−32.9	−2.8
CLECC2020 Δ[%]	−12.3	−30.8	13.0	4.4	−10.2	−16.4	−42.1	−34.0	−5.9
CLECC2030 Δ[%]	−17.6	−35.1	11.8	0.8	−33.2	−20.8	−48.3	−40.8	−7.2
BCAdd2030 Δ[%]	−6.5	−27.2	57.5	37.4	−10.3	−10.9	−40.7	−33.5	−3.6
MTFR2030 Δ[%]	−36.7	−50.4	−59.5	−60.0	−66.3	−39.2	−58.5	−51.5	−15.9

ACPD
14, 31899–31942, 2014

Impacts of emission reductions on aerosol radiative effects

J.-P. Pietikäinen et al.

Table 3. The areal mean forcings for the reference simulation and for the difference between the scenarios and the reference simulation.

	Globe	EU	India	Western China	Eastern China	Africa	Eastern United States	Western United States	South America
DRE									
Refe2005 [$W m^{-2}$]	−3.94	−4.35	−4.16	−2.01	−5.16	−4.08	−3.97	−2.36	−3.59
CLEC2020 Δ[$W m^{-2}$]	0.13	0.56	−0.33	−0.04	0.07	0.16	0.90	0.51	0.05
CLEC2030 Δ[$W m^{-2}$]	0.11	0.54	−0.84	−0.20	0.29	0.15	0.95	0.54	0.03
CLECC2020 Δ[$W m^{-2}$]	0.16	0.61	−0.13	0.03	0.36	0.17	0.98	0.55	0.05
CLECC2030 Δ[$W m^{-2}$]	0.24	0.70	0.04	0.15	1.18	0.25	1.15	0.68	0.06
BCAdd2030 Δ[$W m^{-2}$]	0.06	0.51	−1.32	−0.60	0.12	−0.03	0.94	0.51	0.01
MTFR2030 Δ[$W m^{-2}$]	0.40	0.95	1.15	0.51	2.38	0.31	1.31	0.76	0.13
CRE									
Refe2005 [$W m^{-2}$]	−48.10	−51.05	−33.61	−37.14	−55.61	−31.55	−38.64	−33.87	−55.39
CLEC2020 Δ[$W m^{-2}$]	0.25	1.21	−0.10	−0.04	0.20	0.15	0.69	0.87	0.05
CLEC2030 Δ[$W m^{-2}$]	0.25	1.26	−0.16	−0.11	0.33	0.14	0.75	0.94	0.00
CLECC2020 Δ[$W m^{-2}$]	0.29	1.23	−0.02	0.07	0.26	0.17	0.76	0.89	0.03
CLECC2030 Δ[$W m^{-2}$]	0.38	1.42	−0.02	0.07	0.75	0.25	0.95	1.05	0.05
BCAdd2030 Δ[$W m^{-2}$]	0.38	1.59	0.18	0.24	1.07	0.40	0.78	1.02	0.18
MTFR2030 Δ[$W m^{-2}$]	0.82	2.51	0.98	0.98	2.77	0.70	1.47	1.72	0.55

ACPD
14, 31899–31942, 2014

Impacts of emission reductions on aerosol radiative effects

J.-P. Pietikäinen et al.

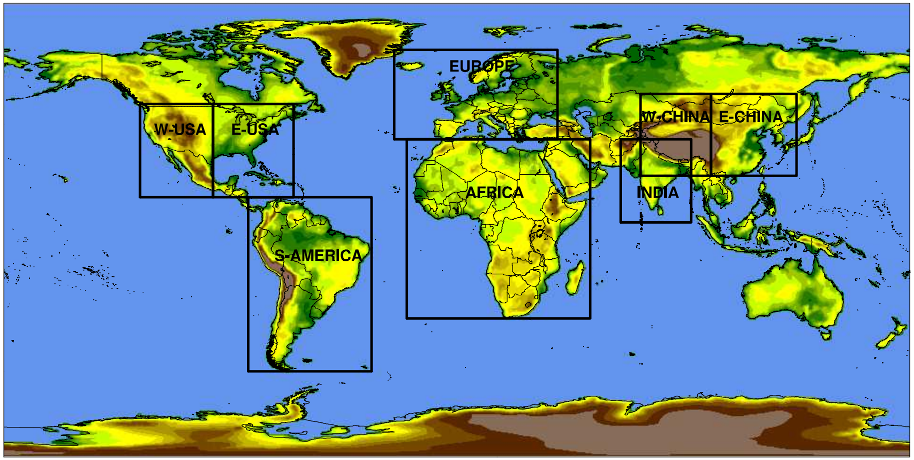

Figure 1. The separately analysed areas: Western United States (W-USA), Eastern United States (E-USA), South America (S-America), Europe, Africa, India, Western China (W-China) and Eastern China (E-China).

ACPD
14, 31899–31942, 2014

Impacts of emission reductions on aerosol radiative effects

J.-P. Pietikäinen et al.

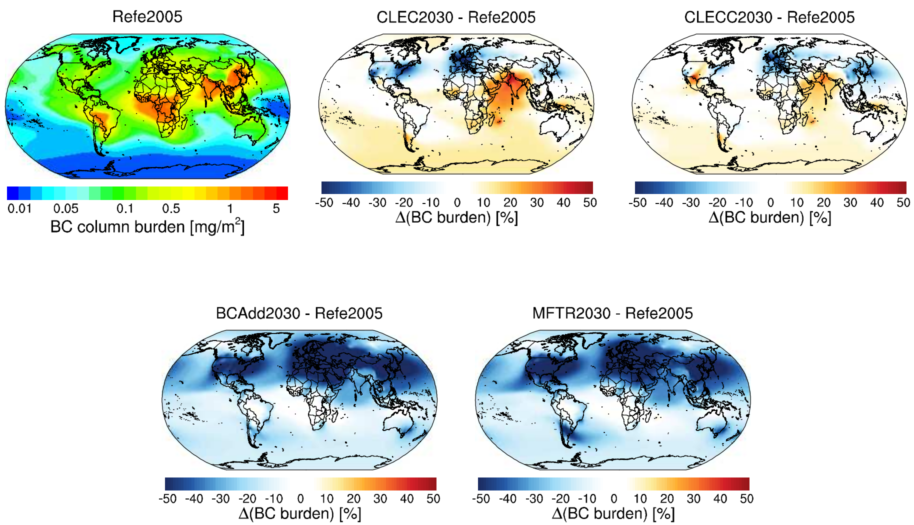

Figure 2. The annual mean BC burden from the reference run and the relative differences between the scenarios and the reference run.

ACPD
14, 31899–31942, 2014

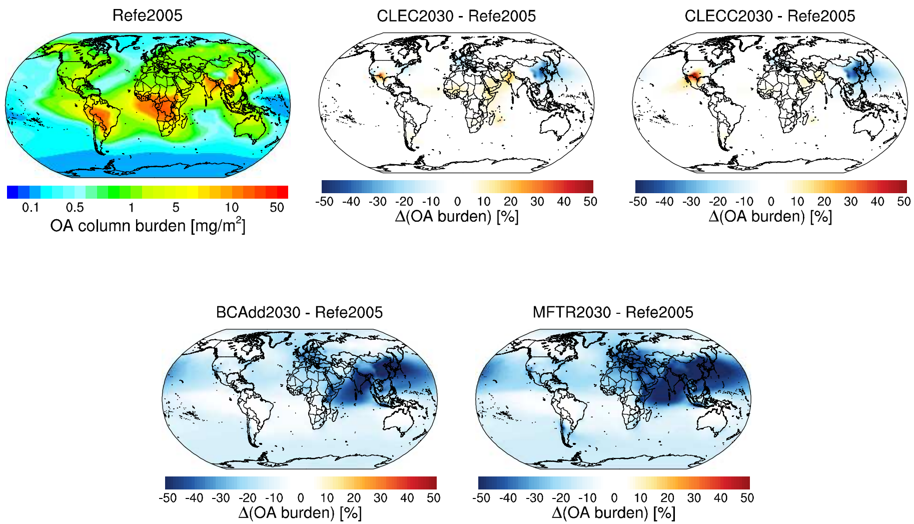

Figure 3. Like Fig. 2, but for OA burden.

ACPD
14, 31899–31942, 2014

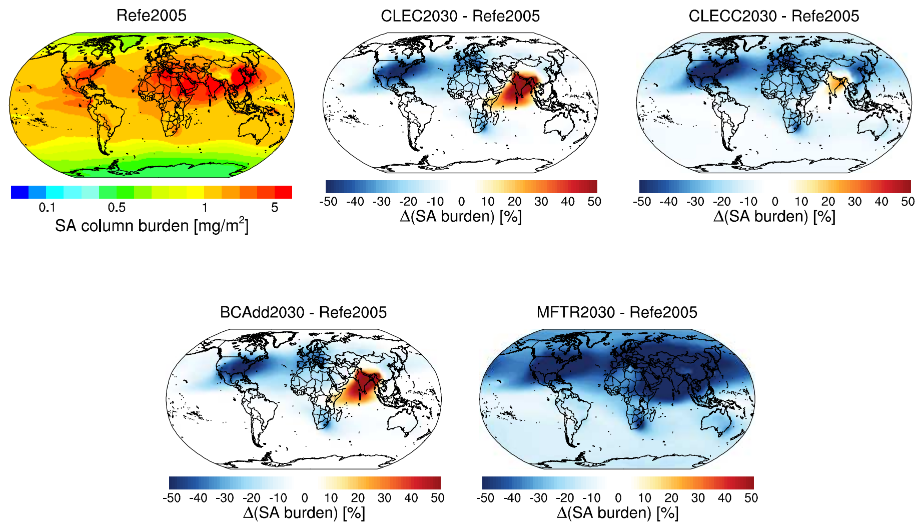

Figure 4. Like Fig. 2, but for SA burden.

ACPD
14, 31899–31942, 2014

Impacts of emission reductions on aerosol radiative effects

J.-P. Pietikäinen et al.

Title Page
Abstract Introduction
Conclusions References
Tables Figures
◀I ▶I
◀ ▶
Back Close
Full Screen / Esc
Printer-friendly Version
Interactive Discussion

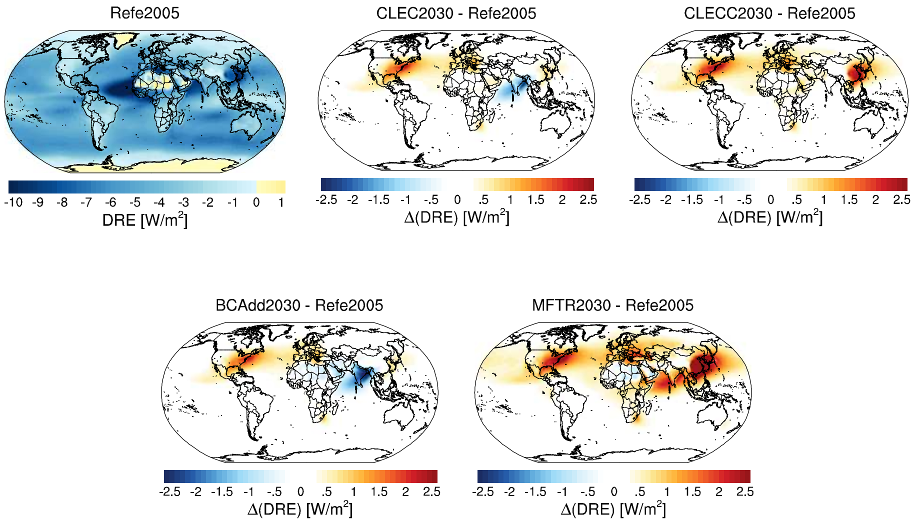

Figure 5. The yearly mean clear-sky DRE at the top of the atmosphere (TOA) from the reference run and the difference between scenarios and the reference run.

ACPD
14, 31899–31942, 2014

Impacts of emission reductions on aerosol radiative effects

J.-P. Pietikäinen et al.

Title Page
Abstract Introduction
Conclusions References
Tables Figures
◀ ▶
Back Close
Full Screen / Esc
Printer-friendly Version
Interactive Discussion

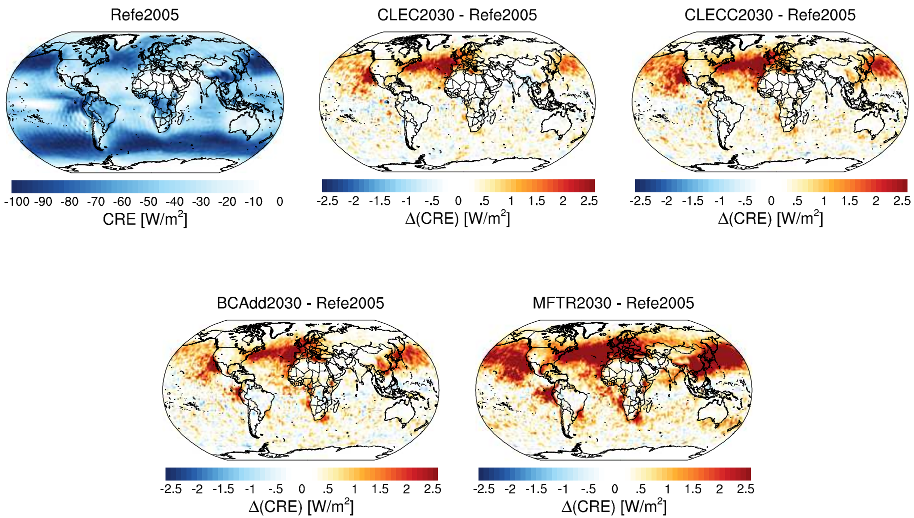

Figure 6. The yearly mean CRE at the top of the atmosphere (TOA) from the reference run and the difference between scenarios and the reference run.

ACPD
14, 31899–31942, 2014

Impacts of emission reductions on aerosol radiative effects

J.-P. Pietikäinen et al.

Title Page
Abstract | Introduction
Conclusions | References
Tables | Figures
Back | Close
Full Screen / Esc
Printer-friendly Version
Interactive Discussion